*This is a non-peer reviewed preprint submitted to EarthArXiv on 30 September 2022*

# Global groundwater warming

Susanne A. Benz[1,2,*], Dylan J. Irvine[3], Gabriel C. Rau[4], Peter Bayer[5], Kathrin Menberg[6], Philipp Blum[6], Rob C. Jamieson[1], Christian Griebler[7], Barret L. Kurylyk[1,*]

[1]Centre for Water Resources Studies, Dalhousie University, Halifax, Canada
[2]Institute of Photogrammetry and Remote Sensing, Karlsruhe Institute of Technology, Karlsruhe, Germany
[3]Research Institute for the Environment and Livelihoods, Charles Darwin University, Casuarina, Australia
[4]School of Environmental and Life Sciences, The University of Newcastle, Newcastle, Australia
[5]Department of Applied Geology, Martin Luther University Halle-Wittenberg, Halle, Germany
[6]Institute of Applied Geosciences, Karlsruhe Institute of Technology, Karlsruhe, Germany
[7]Department of Functional & Evolutionary Ecology, University of Vienna, Vienna, Austria
*Corresponding authors: susanne.benz@dal.ca; barret.kurylyk@dal.ca

## Abstract

Aquifers contain the largest store of unfrozen freshwater, making groundwater critical for life on Earth. Groundwater temperatures influence stream thermal regimes, groundwater-dependent ecosystems, aquatic biogeochemical processes, water quality, and the geothermal potential. Yet little is known about how groundwater responds to surface warming across spatial and temporal scales. We simulate current and projected groundwater temperatures at the global scale and show that groundwater at the depth of the water table is projected to warm on average by 3.3°C between 2000 and 2099 (RCP 8.5). However, regional groundwater warming patterns vary substantially due to spatial variability in climate and water table depth. The highest warming rates are projected in Central Russia, Northern China, and parts of North America and the Amazon rainforest. Results also show that by 2099, 234 million people are projected to live in areas where groundwater exceeds the highest threshold for drinking water temperatures set by any country.

# Introduction

Human activities have rapidly increased the concentration of atmospheric greenhouse gasses since the beginning of the industrial revolution (1). The earth's climatic system warms holistically in response to the resulting radiative imbalance, with the ocean absorbing most of this additional heat (2, 3). However, the terrestrial subsurface also functions as a heat sink in response to climate change. With a stable climate, seasonal temperature variation penetrates to a depth of 10–20 m, below which temperatures increase with depth in accordance with the geothermal gradient (4). However, present-day borehole temperature-depth profiles frequently show an inversion (i.e., temperature decreasing with depth) for up to 100 m due to recent, decadal surface warming (5–8). Deviations from steady-state subsurface temperatures in deep boreholes (e.g., >300 m) have been used to estimate past surface temperature changes at a global scale (9, 10). While multi-continental synthesis studies on subsurface warming provide critical information on climate dynamics, past large-scale studies have never considered impacts of subsurface warming on groundwater resources and associated implications.

With the advent of the GRACE satellites, global datasets, and global hydrological models, there is an emerging body of global-scale groundwater research (11–14). However, global-scale groundwater studies so far have focused on resource quantity (e.g., levels, recharge rates, and gravity signals), while global-scale research into groundwater quality, including temperature, is lacking. Furthermore, prominent syntheses of the relationship between anthropogenic climate change and groundwater (e.g. (15, 16)) concentrate on quantity leaving quality aspects unexplored (17). Water temperature, sometimes known as the 'master environmental variable' (18), is an understudied groundwater quality consideration in the context of climate change.

While global studies of river and lake warming were conducted (19–22), there are no global assessments of climate change impacts on groundwater temperatures (GWTs) or GWTs themselves with the exception of a previous study from *Benz et al.* (2017) estimating multi-annual mean

GWTs (2000 - 2015) independent of depth using an empirical model (23). This is despite the fact that groundwater represents the largest global reservoir of unfrozen freshwater (24), provides at least part of the water supply for half the word (25) and close to half of the global irrigation demand (26), and sustains terrestrial and aquatic ecosystems (27), particularly in the face of climate change (15). Given the role of temperature as an overarching water quality variable and recent observational evidence of groundwater warming in different countries in response to recent climate change (5, 28–32), the potential impacts of climate warming on groundwater temperatures at a global scale remains a critical knowledge gap.

Groundwater temperature influences a suite of biogeochemical processes that alter groundwater quality (33). For example, an increase in temperatures reduces gas solubility and raises metabolism of organisms, with an increased rate of oxygen consumption and a shift in redox conditions (34). Because many aquifers already possess low oxygen concentrations, a small change in temperature could trigger a shift from an oxic to a hypoxic or even an anoxic regime (35, 36). This switch can in turn facilitate the mobilisation of redox-sensitive constituents such as arsenic, manganese, and phosphorus (37–39). Increases in soluble phosphorus in groundwater discharging to surface water can trigger harmful algal blooms (40), and elevated arsenic and manganese contents in potable water supplies pose direct risks to human health (41). An elevation of groundwater temperatures will also cause a shift in groundwater community composition with a challenge to biodiversity and the risk of an impaired cycling of carbon and nutrients (35, 36, 42, 43).

Shallow soil and groundwater warming may also cause temperatures in water distribution networks to cross critical thresholds, with potential health implications such as as the growth of pathogens like *Legionella spp* (44). Discharge of thermally stable groundwater to surface water bodies modulates their thermal regimes (44). If groundwater discharge is focused, warmed groundwater inflows can impact what would otherwise be cold-water zones in the river channel or sediment that provided thermal refuge for stressed aquatic species (45), including many prized cold-water fish. Spring ecosystems will also be affected. For example, crenobionts (true spring water

species) have a very narrow temperature optimum and tolerance, hence warming groundwater, and associated warming of springs will lead to changes in their reproduction cycles, food web interactions, and finally a loss of sensitive species (46).

Groundwater warming can also have positive effects as the accumulated thermal energy can be recycled through shallow, low-carbon geothermal energy systems (47, 48). While studies typically focus on recycling the waste heat from anthropogenic sources, particularly from subsurface urban heat islands (49–51), the subsurface heat accumulating due to climate change also has the potential to sustainably satisfy local heating demands (52). However, increased warming will make cooling systems less efficient (53).

Here, we develop and apply the first global-scale groundwater temperature model and associated online application to quantify aquifer thermal patterns in space and time and their response to recent and projected climate change (Fig. 1a and b). Our objective is to reveal the long-term implications of ongoing shallow groundwater warming and to identify 'hot spots' that are regions of concern. The model utilises standard climate projections to drive global groundwater warming with a focus on temperatures at the depth of the water table. We then discuss (1) where aquifer warming will influence the viability of shallow geothermal heat recycling in the shallow subsurface (Fig. 1c), (2) given how it impacts microbial activity and groundwater chemistry, where groundwater temperature may cross key thresholds set by drinking water standards (Fig. 1d), and (3) where discharge of warmed groundwater will have the most pronounced impact on river temperatures (Fig. 1e).

# Results and Discussion

We use gridded data to calculate transient subsurface temperature-depth profiles across the globe (see Methods). Besides past and current temperatures, we present projections based on the RCP

4.5 or RCP 8.5 climate scenarios of CMIP5 (54). Our global results can be accessed and visually explored using an interactive Google Earth Engine App available under `https://susanneabenz.users.earthengine.app/view/subsurface-temperature-profiles`. Figure 2a displays a global map of annual mean groundwater temperatures at the depth of the water table for 2020.

We use two different datasets to test the accuracy of our global model (see Methods): (1) A dataset of (multi-) annual mean groundwater temperatures (9,967 locations) and (2) individual borehole temperature profiles (72 locations). Overall, the accuracy of our model is good, with a root mean square error of 1.4°C and a coefficient of determination of 0.75 (Fig. 2b). However, errors are not distributed equally across the globe (Supplementary Fig. 1). Groundwater temperatures (GWTs) are for example disproportionally underestimated in the European alpine regions and disproportionally overestimated in Ontario, Canada (Supplementary Fig. 2). However, we find no correlation between model error and thermal diffusivity or latitude (Supplementary Fig. 3). The model performs best in moderate temperatures, underestimating the warmest and overestimating the coldest locations of both datasets used for evaluation. In populated areas, GWT are also underestimated as they are highly impacted by anthropogenic influences such as surface sealing, subsurface infrastructure and urban heat discharge, which are not adequately represented in our model or input data (Supplementary Fig. 3).

The median GWT in 2020 was 14.9°C (1.9°C, 28.7°C; 10th, 90th percentile, Fig. 2a). In comparison, using the same ERA-5 data product, air temperatures in 2020 were lower at 12.0°C (-7.7°C, 26.7°C). This thermal offset is attributable to various processes and conditions including increased temperatures with depth following the geothermal gradient. In colder climates it is also due to snow pack insulation at higher latitudes (55). For many locations, GWTs at the water table show no seasonal variation (Supplementary Fig. 4). However, in parts of Canada, Siberia, and other regions with shallow water tables (or at locations where wetlands are an expression of the water table), pronounced seasonal variations are found and GWT can vary by >10°C over the year. This large temperature variation between climates and localities is also evident in the time series

of six example locations distributed over a broad range of latitudes in Supplementary Fig. 5: The locations in China, Nigeria, and Norway with groundwater levels of <5 m below ground surface show seasonal variations Supplementary Fig. 5). In contrast, the selected stations in Australia, Brazil, and Mexico, where the depth to the groundwater level is 30 m or more, exhibit no seasonal trends.

Simulated temperature-depth profiles are displayed at these six example locations in Fig. 2c. While all locations show an inversion of the temperature-depth profile, the depth at which this thermal gradient "inflection point" is reached varies greatly based on the rate and duration of recent climate change. In our location considered in Mexico, temperatures begin to increase with depth (as expected based on the local geothermal gradient) from approximately 10 meters downwards, whereas in our location in Brazil, the inflection point reaches as dept of 45 m (Fig. 2c). Globally, it has reached 15 (<1, 40) meters (Supplementary Fig. 6a). Heat advection from vertical groundwater flow may also influence the depth of the inflection point (5), but only heat diffusion is considered in our model (see Methods)

To better assess the impact of recent climate change on groundwater temperatures, we compare annual mean GWTs from 2000 and 2020 at the water table depth. Over this 20-year period, GWTs increased on average by 0.3 (0.0, 0.9) °C (Fig. 3a). Some of the highest temperature increases occur in parts of Russia (e.g., >+1.5 °C north of Novosibirsk) while parts of Canada experienced cooling (e.g., <-0.5 °C in Saskatoon) between the two years. Both regions have shallow groundwater, with GWTs tightly coupled to seasonal surface temperature variations and short-term intra-annual changes, rather than the long-term surface temperature signals. As such, one hot summer can drastically alter the modelled GWT difference between 2000 and 2020. Accordingly, here groundwater warming is not uniform over the seasons (Supplementary Fig. 7).

The influence of weather conditions for a given year on shallow subsurface temperatures is also notable in the depth profiles for the six selected locations (Fig. 3d). Significant variations

occur in the upper 5 m of mean temperature range profiles with temperature changes of 1.1°C at our location in Australia, compared to 0.5°C at our location in Nigeria. Differences between mean annual temperatures at 5 m depth for two different years may be caused interannual or intra-annual temperature changes, rather than climate change. The effects of intra-annual and short-term interannual variations in weather are attenuated at greater depths (e.g. 30 m). However, long-term (climate change) effects are transported to great depths, although groundwater warming may be less pronounced with depth due to the time lag between surface and subsurface temperature signals (Fig. 3c).

Warming is projected to continue with globally averaged GWT increasing by 3.3 (1.0, 5.0)°C between 2000 and 2099 following RCP 8.5 median projections (Fig. 3e-g; Supplementary Fig. 8 for 10th and 90th percentile projections) and by 1.7 (0.8, 2.5)°C following RCP 4.5 (Supplementary Figs. 9a-d and 10). Highest warming rates are primarily located in Central Russia, Northern China, the Midwest of the US, the Canadian Prairies, and parts of the Amazon rain forest in Brazil and Peru. In addition, warming is not uniform over the seasons (Supplementary Figs. 11 and 12), and seasonal variations in GWT will change (Supplementary Fig. 13). In the Northern Hemisphere, warming is often more pronounced in the early summer, and we see a greater increase in GWT maxima than minima. In parts of Canada and Russia, where the water table is very shallow (e.g., <5 m), our results even project some cooling following RCP 4.5 during October and November (Supplementary Fig. 12 j and k). Due to the shallow groundwater level at these locations, this is again more an indication of different summer air temperatures in 2000 and 2099 rather than a long-term trend. However, we observe a much clearer signal of climate change by studying the depth down to which the temperature profile is inverted and temperatures are decreasing outside of seasonal effects. In 2099 geothermal gradient inflection point is projected to reach 60 (35, 100) m on average following RCP 8.5 or 35 (5, 80) m following RCP 4.5 (Supplementary Fig. 6b and c).

The overall increase in GWT can be quantified as accumulated energy (see Methods). By 2020, $17 \times 10^{21}$ J have already been absorbed by the terrestrial subsurface (Fig 4a, 125 (53,

215) $MJm^{-2}$) since the beginning of the industrial revolution. In comparison, $436 \times 10^{21}$ J or about 25 times more has been absorbed by the oceans over a similar time period (56). A review of the Earth energy imbalance identifies a total heat gain of $358 \times 10^{21}$ J for the time period 1971–2018 only, attributing about 6% of that to land areas ($21 \times 10^{21}$ J, slightly more but of similar magnitude as our estimate) (57). We project that by 2099 accumulated subsurface energy will be $67 \times 10^{21}$ J following RCP 8.5 (497 (372, 673) $MJm^{-2}$, Fig 4d) and $43 \times 10^{21}$ J following RCP 4.5 (328 (233, 451) $MJm^{-2}$, Supplementary Fig. 9e). This accumulated heat can be extracted from the subsurface through wells in productive aquifers, in lower-permeability zones and the unsaturated zone less efficient borehole heat exchangers are necessary (47). Hence, we assessed the energy accumulated in the saturated zone only (i.e., below the water table) in Supplemental Fig. 14 - on average there are 75 (15, 151) $MJm^{-2}$ in the aquifer in 2020.

By comparing the accumulated thermal energy in the aquifer of the US (about 45 $MJm^{-2}$) with local residential heating demands (about 35,000 MJ per household in 2015 following the U.S. Energy Information Administration 2015 Energy Consumption Survey) we find that, if recycled, the energy accumulated below an average home (250 $m^2$ for the floor area in new single-family houses following the 2015 "Characteristics of new housing" report, U.S. Department of Commerce) would fulfill about 4 month of heating demands. However, by 2099, global heat storage in the saturated zone is projected to increase to 225 (75, 369) $MJm^{-2}$ following RCP 4.5 and 342 (108, 545) $MJm^{-2}$ following RCP 8.5 (Supplemental Fig 14). With heating demands projected to decline due to warmer temperatures and improved building insulation, recycling this subsurface heat will therefore become more feasible and is a carbon-reduced heat source that will benefit from climate change (52). Conversely, cooling systems that rely on geothermal sources will be less efficient.

While groundwater warming has positive benefits for heating with geothermal systems, the accumulated heat also threatens groundwater quality. In many developing countries or in poor or rural areas within developed countries, untreated groundwater may be consumed directly without treatment. In these regions in particular, the changes in water chemistry or microbiology that are

associated with groundwater warming, such as increased risk for pathogen growth in distribution systems, has to be carefully considered. According to the World Health Organization (WHO), only 18 of 125 countries have temperature guidelines for drinking water (58). These temperature guidelines, which are often aesthetic guidelines, range from 15 °C to 34 °C, with a median of 25°C. Fig 4b shows where annual maximum groundwater temperatures are above these thresholds in 2020. At this time, more than 30 million people live in areas where our modeled GWT exceed 34°C. Following RCP 4.5 and the shared socioeconomic pathway (SSP) *Middle of the Road* (59, 60), by 2099, this number will increase to more than 88 million. Following RCP 8.5 and the SSP *Fossil-fuelled Development (Taking the Highway)*, more than 234 million people will live in areas, where GWT exceed the highest thresholds for drinking water temperatures due to groundwater warming and changes in population.

The ecosystems most dependent on groundwater are the aquifers themselves (61). A temperature increase will challenge groundwater biodiversity and ecosystem services (62, 63) and the increased metabolic rates of microbes caused by warming will accelerate the cycling of organic and inorganic matter, additionally fueled by the increasing import of dissolved organic carbon to the subsurface (64). Combined with decreasing groundwater recharge as projected for many North African, Southern European, and Latin American countries (65), this poses a risk for turning oxic into anoxic subsurface environments (35).

Groundwater warming also threatens many riverine groundwater-dependent ecosystems and the industries (e.g., fisheries) that they support. To capitalize on past continental-scale research related to groundwater, river temperature, and ecosystems, we compare our modelled spatial patterns of groundwater warming in the conterminous US to a recent distributed analysis of 1,729 stream sites (66). The amplitude and phase of seasonal temperature signals in these surface water bodies was used to reveal the thermal influence and source depth of groundwater discharge to these streams, with about 40% classified as groundwater-dominated. Our results show that GWT at the groundwater-dominated stream sites increased by 0.1 (0.0, 0.4)°C between 2000 and 2020

and 0.6 (0.2, 1.1)°C and 1.1 (0.2, 2.6)°C between 2000 and 2099 following RCP 4.5 and RCP 8.5, respectively (Fig. 4c and f, and Supplementary Fig 9g).

The warming groundwater will inevitably raise the ambient temperature of surface water systems thermally influenced by groundwater discharge. Furthermore, such groundwater warming will strongly impact the thermal regimes of groundwater-fed thermal refuges (e.g., springs or groundwater-dominated tributaries flowing into rivers) by causing them to more regularly cross critical temperature thresholds for resident species seeking relief from thermal stress. Given the connection between aquifer thermal regimes and river sediment temperatures (67), groundwater warming also threatens the thermal suitability of benthic ecosystems and spawning areas for fish (68), posing a major risk to fisheries and other dependent industries.

In summary, global climate change is leading to increased atmospheric and surface water temperatures, both of which were assessed across spatial scales ranging from local to global. Here we contribute to the global analyses of environmental temperature change and of groundwater resources through the presentation of projected groundwater temperature change to 2100 at a global scale. Our analyses allow for both the hindcasting and forecasting of groundwater temperatures. Future groundwater temperature forecasts are based on both RCP 4.5 and 8.5 climate scenarios. We provide global temperature maps at the depth of the water table, 5 and 30 m below land surface, and these highlight that places globally with shallow water tables and/or high rates of atmospheric warming will experience the highest groundwater warming rates.

To facilitate more detailed future analyses, the temperature maps are included in a Google Earth Engine app under `https://susanneabenz.users.earthengine.app/view/subsurface-temperature-profiles`. The gridded GWT output could be integrated with global river temperature models (i.e. (20)) to more holistically understand future warming in connected aquifers and rivers. While the warming of the earth's groundwater poses some opportunities for geothermal energy production, groundwater warming poses far more, often significant risks.

Warming groundwater could threaten many groundwater-dependent ecosystems and the industries depending on them, and will lead to negative impacts on drinking water quality, primarily in less developed regions.

# Methods

## Diffusive Heat Transport

We model monthly subsurface temperatures (and therefore also groundwater temperatures (GWTs)) from the surface to a depth of 100 m for the years 2000 to 2020 as well as future projections following RCP 4.5 and RCP 8.5 up to 2099. Subsurface temperatures in the shallow crust are generally controlled by one-dimensional (vertical) diffusive heat transport. Heat advection due to water flow plays a lesser and often inconsequential role in controlling subsurface temperatures (69–71). The assumption of the dominant role of diffusion underlies many of the global earth system models as well as all of the standard thermal analysis approaches in the field of borehole climatology (69) and some past local studies of groundwater warming (e.g., (72)). Given the global scale for the present study, only a parsimonious modelling approach was tractable. We do not consider advection due to (1) the aforementioned general dominance of diffusion and (2) the challenges with obtaining reasonable advection-influenced temperature-depth profiles for steady-state initial conditions given the profile curvature caused by advection (73). Starting simulations with inappropriate initial temperature conditions can yield much greater errors when simulating GWT than assuming heat transfer is dominated by diffusion (74). A discussion of the impacts of advection is given in the Supplementary Information.

To ensure our initial conditions for temperature-depth profiles are also not influenced by any preceding climate change, we initiate our model in 1880 when the industrial revolution had not yet increased greenhouse gasses in our atmosphere and the climate was stable. For our initial condition, we use a temperature-depth profile that increases linearly with depth $z$ from the temperature at the surface $T_S$ in accordance with the geothermal gradient $a$: $T(z) = T_S + a \cdot z$ (70). In permafrost regions, warming above critical thresholds requires latent heat to thaw ground in addition to the sensible heat to raise the temperature. As we do not include latent heat effects, model results in

permafrost regions (75) are therefore denoted with hatching in our figures to highlight the high uncertainties in predictions.

We use the following analytical solution to the transient, 1D heat diffusion equation for a semi-infinite homogeneous medium subject to a series of $n$ step changes in surface temperature (70):

$$T(t,z) = T_S(t=0) + az + \sum_{t_j=1}^{t_j<t} \Big(T_S(t_j) - T_S(t_{j-1})\Big) \cdot erfc\left(\frac{z}{2\sqrt{D \cdot (t_j - t_{j-1})}}\right) \quad (1)$$

where $j$ is a step change counter (counting by month), $t$ is time, $T_S(t)$ is the time series of the ground surface temperature, $D$ is the thermal diffusivity, and $erfc$ is the complementary error function.

We run our model in Google Earth Engine (GEE) (76), and the results are presented in the form of a Google Earth Engine App openly accessible under `https://susanneabenz.users.earthengine.app/view/subsurface-temperature-profiles`. The application presents zoomable maps of annual mean, maximum, and minimum GWT at different depths as well as seasonal variability (maximum minus minimum) for selected years and climate scenarios. All datasets were created at a native 5 km resolution at the earth's surface. However, Google Earth Engine automatically rescales images shown on the map based on the zoom level of the user. By clicking on the map, charts that represent temperatures at that location at a 5 km scale are created and can be exported in CSV, SVQ or PNG file formats. For all analyses showing annual mean data at the water table depth, we first calculate monthly temperatures at the monthly groundwater level before averaging the results.

## Ground Surface Temperatures

We use two distinct ground surface temperature time series: (1) one for our analysis of current (2020) temperatures based primarily on the ERA-5 data (77) and (2) one for our analysis of

projected changes based on CMIP5 data (54). Based on available computational power and data we are not able to utilize monthly temperatures for the entire time period between the years 1880 and 2099. Instead, we present monthly temperatures from 1981 onwards and annual mean temperatures of 1880. As these data are input into the analytical step function model model (Eq. 1), we supplement them with mean temperatures of the early 1980s (i.e., 3-year mean 1981 to 1984). An example of the ground surface temperature time series is shown in Supplementary Fig. 15.

For our analysis of current GWT we use monthly mean soil temperature at 0-7 cm depth for the years 1981 to 2022 based on the ERA-5-Land monthly average reanalysis product (77) to form the ground surface temperature boundary condition for Eq. 1. These data have a native resolution of 9 km at the surface and are available through the Google Earth Engine (GEE) data catalog. We also used annual ground temperature anomalies of 1880 of the top layer following the GISS atmospheric model E (78). This dataset gives the temperature difference between 1880 and 1980 in a horizontal resolution of $4^\circ \times 5^\circ$ (approx. 444 km $\times$ 555 km at the equator) and can be extracted from `https://data.giss.nasa.gov/modelE/transient/Rc_ij.1.11.html`. To obtain absolute temperatures of 1880, we subtract the anomalies from 3-year mean temperatures (1981 to 1984) of the ERA-5 data.

Future projections of ground surface temperatures are based on monthly soil temperatures closest to the surface for scenarios RCP 4.5 and RCP 8.5 from the CMIP5 program available from 2006 to 2099 (54). Model selection and methodology follow previous work (52, 79) in using the models BCC-CSM1-1, BNU-ESM, CanESM2, CCSM4, INM-CM4, IPSL-CM5A-LR, MIROC5, MPI-ESM-LR, MRI-CGCM3, and NorESM1-M. Data were collected from the World Climate Research Program at `https://esgf-node.llnl.gov/search/cmip5/`. In addition, monthly data of the historic scenario were prepared for January 1981 to December 2005 and the annual mean data for 1880. To account for the difference between the CMIP5 models and ERA-5 reanalysis, we adjust the CMIP5 outputs based on mean temperatures $\overline{T}$ from ERA-5 between 1981 and 2006 (i.e., the overlap between ERA-5 and the CMIP5 historic scenario) for each of the CMIP5 models

separately as follows:

$$T_{CMIP5,adjusted}(t) = T_{CMIP5}(t) - \overline{T}_{CMIP5}(1981 \leq t < 2006) + T_{ERA5}(1981 \leq t < 2006). \quad (2)$$

Temperatures are determined for each model before being presented as the median and the 10th and 90th percentiles.

## Thermal Diffusivity

For our analysis we use the ground thermal diffusivity $D$:

$$D = \frac{\lambda}{C_V}, \quad (3)$$

where $\lambda$ ($Wm^{-1\circ}C^{-1}$) is thermal conductivity and $C_V$($Jm^{-3\circ}C^{-1}$) is volumetric heat capacity of the unsaturated zone. Ground thermal conductivity and volumetric heat capacity for various water saturation values are derived following previous examples (52, 80). This method links $\lambda$ and $C_V$ values for different soil and/or rock types following the *VDI 4640* guidelines (81) to a global map of soil and/or rock type. This map is based on grain size information of the unconsolidated sediment map database (GUM) (82). Where there is no available sediment class, we link to soil type in GUM. Where this is also not available, we rely on the global lithological map database (GLiM) (83).

All required datasets were uploaded to Google Earth Engine in their native resolution. For assigned values, refer to Supplementary Table 1. Overall, thermal properties are well constrained (84). We note that water saturation can change the individual thermal properties and have accordingly run our model for six example locations with three different diffusivity values: (1) dry soil, (2) a moist soil (default) and (3) a water saturated soil (Supplementary Fig. 16). The influence of soil moisture on thermal diffusivity can be complex as both the heat capacity and thermal

conductivity increase with water content (Eq. 3). Overall, for locations with unconsolidated material in the shallow subsurface, groundwater warming rates increase with water saturation. However, the effect is non-linear and the overall impact of water saturation on the thermal diffusivity is negligible for relative saturation values between 0.5-1 (85). A map of the diffusivity utilized here is given in Supplementary Fig. 17a.

## Geothermal Gradient

The geothermal gradient $a$ ($^{\circ}Cm^{-1}$ see Eq. 1) is the rate of temperature change with depth due to the geothermal heat flow $Q$ ($Wm^{-2}$) and thermal conductivity $\lambda$ ($Wm^{-1\circ}C^{-1}$):

$$a = \frac{Q}{\lambda} \tag{4}$$

with global values for $\lambda$ derived as described earlier, and the mean heat flow $Q$ available as a global 2° equal area grid (about 222 km at the equator)(86). The grid was uploaded to GEE in its native resolution for analysis (Supplementary Fig. 17b).

## Water Table Depth

Much of our analysis and interpretation focuses on the future projection of temperatures at the water table depth. We therefore use the results of a previously published global groundwater model (87, 88) with a 30 sec grid (about 1 km at the equator) to obtain the mean water table depth for 2004 to 2014. These data are available as monthly averages that we uploaded to GEE in their native resolution. In temperate climates, the model underestimates the observed water table depth by 1.5 m, and we therefore set the minimum water table depth to 1.5 m as was done in a previous study (52).

To calculate mean annual GWT at the water table, temperatures for each month were determined at the corresponding water table depth by setting $z$ to this depth in Eq. 1. Future changes of water table elevation are challenging to predict, and we therefore base our analysis on the assumption that future water table elevations are unchanging.

## Model Evaluation

To assess the performance of our GWT calculations, we use two datasets of measured GWT or borehole temperatures. First, we compare our data to (multi-)annual mean shallow GWTs introduced in *Benz et al.* (52). These data comprise more than 8,000 individual locations, primarily in Europe, where GWTs were measured at least twice between 2000 and 2015 at less than 60 m depth. Measurements are filtered based on their seasonal radius, i.e., a measure describing if a well was observed uniformly over the seasons and mean temperatures are therefore free of seasonal bias (23). Second, we compare our data to temperature-depth profiles from the Borehole Temperatures and Climate Reconstruction Database at `https://geothermal.earth.lsa.umich.edu/core.html`. For these data, an exact date and depth of measurement are known. We filter the database based on time of measurement and depth of the first measurement, using only data taken after the year 2000 and starting at less than 30 m depth, resulting in 72 borehole measurements. To evaluate the model, we compare it to the observed groundwater temperatures described above. We compare the shallow (multi-)annual mean temperatures to mean temperatures at 30 m depth between 2000 and 2015. For the dataset of one-time borehole temperature-depth profiles, we compare the most shallow data points to temperatures from our model at the same depth (rounded to the nearest meter), month and year. Supplementary Fig. 2 shows comparisons of all depths for the observed temperature depth profiles down to 50 m, highlighting local discrepancies depend on site specific land use, climatic, hydrological and geological variability that are not resolved by the large-scale model. In general, the model performs well (RMSE = 1.8°C for most shallow points

in profiles), but there are discernible errors (e.g., a 5°C difference in temperatures at 1 m depth in the borehole JP-Tateno located in a golf-course near Tokyo where we model a seasonal signal but the observation shows none). However, we would note that our primary goal is to look at large-scale shallow groundwater warming patterns, rather than reproducing absolute temperatures in individual profiles. Still, in Supplementary Fig. 3, we showcase the impacts of latitude, observed GWT, diffusivity and population density (as a proxy for urban heat island effects) on the model error. For this we use the 2015 UN-adjusted population density from the Population of World Version 4.11 Model (89).

## Example Locations

We use six locations distributed over all latitudes as examples in many of our figures: One each in Australia (Longitude: 149.12°, Latitude: -35.28°), Brazil (-47.92°, -15.77°), China (116.39°, 39.90°), Mexico (-99.12°, 19.46°), Norway (10.74°, 59.91°), and Nigeria (7.49°, 9.05°). For convenience, each point is at the location of the capital city. However, as our model is not able to adequately describe the impact of urban heat on measured groundwater temperatures, groundwater at these locations is expected to be warmer, potentially by several degrees.

## Depth of the Thermal Gradient "Inflection Point"

To find the depth $d_i$ down to which subsurface temperatures $T$ are inverted (i.e., decrease with depth as opposed to increase following the geothermal gradient (5)) we find the maximum depth where $T(d_i) > T(d_{i+1})$. Given our computational resources, we test this at a resolution of 1 meter steps for the first 10 m, then in 5 m steps down to 50 m depth, and lastly in 10 m steps down to the maximal depth of 100 m.

## Accumulated Energy

To quantify shallow subsurface accumulated energy $I$ $(Jm^{-2})$, we compare annual mean temperature-depth profiles down to 100 m depth to the initial conditions $T(z) = T_S(t = 1880) + a \cdot z$ as follows:

$$I = \int_{z=0}^{z=100} \Big( \overline{T}(z) - T_S(t = 1880) - az \Big) \cdot C_V(z) dz. \tag{5}$$

This analysis utilizes annual mean subsurface temperatures $\overline{T}(z)$ for 2020 or 2099 for the current and projected analyses, respectively. The volumetric heat capacity $C_V(z)$ of the unsaturated zone (for $z$ above the water table) and the saturated zone (for $z$ below the water table) uses discrete values given in Supplementary Table 1. We solve the integral in 1 m steps.

## Drinking Water Temperature Thresholds

To assess the impact of groundwater warming on its suitability as drinking water, we compare annual maximum groundwater temperatures to thresholds for drinking water temperatures summarized by the World Health Organisation (WHO) (58). To quantify populations at risk of exceeding the threshold, we compare the resulting maps with population counts. For temperatures in 2022 we use the 2015 UN-adjusted population density from the Population of World Version 4.11 Model (89). For future scenarios we rely on the global population projection grids for 2100 from the Shared Socioeconomic Pathways (SSPs) (59, 60). These data are available through the socioeconomic data and applications center (SEDAC). We link the base scenario of SSP5 *Fossil-fuelled Development (Taking the Highway)* to RCP 8.5, and SSP2 *Middle of the Road* to RCP 4.5. For the latter, we must note that some mitigation efforts are necessary for this pathway to not overshoot the projected greenhouse gas concentrations.

## Impact on Surface Water Bodies

Temperatures in surface water bodies are strongly influenced by atmospheric heat fluxes, but groundwater discharge can decouple temperatures in the atmosphere and water column. In the US, 1,729 stream sites have been analyzed by *Hare et al. (2021)* (66) to determine the dominance of groundwater discharge and to ascertain the relative depth (shallow or deep) of the associated aquifers. We use these sites to extract changes in mean annual groundwater temperature at the depth of the water table from our results to assess the impact of groundwater warming on these surface water bodies.

# Data Availability

Raster files (5 km resolution, in the GeoTIF format) and tables (.CSV) used to create all figures of this study are made available at the Scholars Portal Dataverse under `https://doi.org/10.5683/SP3/GE4VEQ`. (For review purposes available under `https://borealisdata.ca/privateurl.xhtml?token=1acd0d10-7591-4126-ad11-49c60f9cbf08`.) Furthermore, we have provided an online tool to facilitate exploration of our groundwater temperature model at `https://susanneabenz.users.earthengine.app/view/subsurface-temperature-profiles`.

# Code Availability

All data and codes will be made available after publication.

# References


[1] Meinshausen, M. *et al.* Historical greenhouse gas concentrations for climate modelling (CMIP6). *Geoscientific Model Development* **10**, 2057–2116 (2017). URL https://doi.org/10.5194/gmd-10-2057-2017.

[2] Arias, P. *et al. Technical Summary - Climate Change 2021: The Physical Science Basis. Contribution of Working Group I to the Sixth Assessment Report of the Intergovernmental Panel on Climate Change*, 33–144 (Cambridge University Press, Cambridge, United Kingdom and New York, NY, USA, 2021).

[3] Meyssignac, B. *et al.* Measuring global ocean heat content to estimate the earth energy imbalance. *Frontiers in Marine Science* **6** (2019). URL https://doi.org/10.3389/fmars.2019.00432.

[4] Kurylyk, B. L. & Irvine, D. J. Heat: An overlooked tool in the practicing hydrogeologist's toolbox. *Groundwater* **57**, 517–524 (2019). URL https://doi.org/10.1111/gwat.12910.

[5] Bense, V. F. & Kurylyk, B. L. Tracking the subsurface signal of decadal climate warming to quantify vertical groundwater flow rates. *Geophysical Research Letters* **44** (2017). URL https://doi.org/10.1002/2017gl076015.

[6] Kooi, H. Spatial variability in subsurface warming over the last three decades; insight from repeated borehole temperature measurements in the netherlands. *Earth and Planetary Science Letters* **270**, 86–94 (2008). URL https://doi.org/10.1016/j.epsl.2008.03.015.

[7] Ferguson, G. & Woodbury, A. D. The effects of climatic variability on estimates of recharge from temperature profiles. *Ground Water* **43**, 837–842 (2005). URL https://doi.org/10.1111/j.1745-6584.2005.00088.x.

[8] Taniguchi, M. *et al.* Disturbances of temperature-depth profiles due to surface climate change and subsurface water flow: 1. an effect of linear increase in surface temperature caused by

global warming and urbanization in the tokyo metropolitan area, japan. *Water Resources Research* **35**, 1507–1517 (1999). URL https://doi.org/10.1029/1999wr900009.

[9] Smerdon, J. E. & Pollack, H. N. Reconstructing earth's surface temperature over the past 2000 years: the science behind the headlines. *WIREs Climate Change* **7**, 746–771 (2016). URL https://doi.org/10.1002/wcc.418.

[10] Pollack, H. N., Huang, S. & Shen, P.-Y. Climate change record in subsurface temperatures: A global perspective. *Science* **282**, 279–281 (1998). URL https://doi.org/10.1126/science.282.5387.279.

[11] Döll, P. & Fiedler, K. Global-scale modeling of groundwater recharge. *Hydrology and Earth System Sciences* **12**, 863–885 (2008). URL https://doi.org/10.5194/hess-12-863-2008.

[12] Famiglietti, J. S. The global groundwater crisis. *Nature Climate Change* **4**, 945–948 (2014). URL https://doi.org/10.1038/nclimate2425.

[13] Wada, Y. *et al.* Global depletion of groundwater resources. *Geophysical Research Letters* **37** (2010). URL https://doi.org/10.1029/2010gl044571.

[14] Gleeson, T., Befus, K. M., Jasechko, S., Luijendijk, E. & Cardenas, M. B. The global volume and distribution of modern groundwater. *Nature Geoscience* **9**, 161–167 (2015). URL https://doi.org/10.1038/ngeo2590.

[15] Taylor, R. G. *et al.* Ground water and climate change. *Nature Climate Change* **3**, 322–329 (2012). URL https://doi.org/10.1038/nclimate1744.

[16] Green, T. R. *et al.* Beneath the surface of global change: Impacts of climate change on groundwater. *Journal of Hydrology* **405**, 532–560 (2011). URL https://doi.org/10.1016/j.jhydrol.2011.05.002.

[17] Rodell, M. *et al.* Emerging trends in global freshwater availability. *Nature* **557**, 651–659 (2018). URL https://doi.org/10.1038/s41586-018-0123-1.

[18] Hannah, D. M. & Garner, G. River water temperature in the united kingdom. *Progress in Physical Geography: Earth and Environment* **39**, 68–92 (2015). URL https://doi.org/10.1177/0309133314550669.

[19] van Vliet, M. T. H., Ludwig, F., Zwolsman, J. J. G., Weedon, G. P. & Kabat, P. Global river temperatures and sensitivity to atmospheric warming and changes in river flow. *Water Resources Research* **47** (2011). URL https://doi.org/10.1029/2010wr009198.

[20] Liu, S. *et al.* Global river water warming due to climate change and anthropogenic heat emission. *Global and Planetary Change* **193**, 103289 (2020). URL https://doi.org/10.1016/j.gloplacha.2020.103289.

[21] Bosmans, J. *et al.* FutureStreams, a global dataset of future streamflow and water temperature. *Scientific Data* **9** (2022). URL https://doi.org/10.1038/s41597-022-01410-6.

[22] O'Reilly, C. M. *et al.* Rapid and highly variable warming of lake surface waters around the globe. *Geophysical Research Letters* **42** (2015). URL https://doi.org/10.1002/2015gl066235.

[23] Benz, S. A., Bayer, P. & Blum, P. Global patterns of shallow groundwater temperatures. *Environmental Research Letters* **12**, 034005 (2017). URL https://doi.org/10.1088%2F1748-9326%2Faa5fb0.

[24] Ferguson, G. *et al.* Crustal groundwater volumes greater than previously thought. *Geophysical Research Letters* **48** (2021). URL https://doi.org/10.1029/2021gl093549.

[25] Zektser, I. S. & Everett, L. G. *Groundwater resources of the world and their use* (UNESCO). OCLC: 137335364.

[26] Siebert, S. *et al.* Groundwater use for irrigation - a global inventory. *Hydrology and Earth System Sciences* **14**, 1863–1880 (2010). URL https://doi.org/10.5194/hess-14-1863-2010.

[27] de Graaf, I. E. M., Gleeson, T., van Beek, L. P. H. R., Sutanudjaja, E. H. & Bierkens, M. F. P. Environmental flow limits to global groundwater pumping. *Nature* **574**, 90–94 (2019).

[28] Chen, C.-H. *et al.* Comparisons between air and subsurface temperatures in taiwan for the past century: A global warming perspective. In *Groundwater and Subsurface Environments*, 185–199 (Springer Japan, 2011). URL https://doi.org/10.1007/978-4-431-53904-9_10.

[29] Figura, S., Livingstone, D. M., Hoehn, E. & Kipfer, R. Regime shift in groundwater temperature triggered by the arctic oscillation. *Geophysical Research Letters* **38**, n/a–n/a (2011). URL https://doi.org/10.1029/2011gl049749.

[30] Hemmerle, H. & Bayer, P. Climate change yields groundwater warming in bavaria, germany. *Frontiers in Earth Science* **8** (2020). URL https://doi.org/10.3389/feart.2020.575894.

[31] Menberg, K., Blum, P., Kurylyk, B. L. & Bayer, P. Observed groundwater temperature response to recent climate change. *Hydrology and Earth System Sciences* **18**, 4453–4466 (2014). URL https://doi.org/10.5194/hess-18-4453-2014.

[32] Benz, S. A., Bayer, P., Winkler, G. & Blum, P. Recent trends of groundwater temperatures in austria. *Hydrology and Earth System Sciences* **22**, 3143–3154 (2018). URL https://doi.org/10.5194/hess-22-3143-2018.

[33] Riedel, T. Temperature-associated changes in groundwater quality. *Journal of Hydrology* **572**, 206–212 (2019). URL https://doi.org/10.1016/j.jhydrol.2019.02.059.

[34] Cogswell, C. & Heiss, J. W. Climate and seasonal temperature controls on biogeochemical transformations in unconfined coastal aquifers. *Journal of Geophysical Research: Biogeosciences* **126** (2021). URL https://doi.org/10.1029/2021jg006605.

[35] Griebler, C. *et al.* Potential impacts of geothermal energy use and storage of heat on groundwater quality, biodiversity, and ecosystem processes. *Environmental Earth Sciences* **75** (2016). URL https://doi.org/10.1007/s12665-016-6207-z.

[36] Retter, A., Karwautz, C. & Griebler, C. Groundwater microbial communities in times of climate change. *Current Issues in Molecular Biology* **41**, 509–538 (2021).

[37] Erickson, M. L. *et al.* Machine learning predicted redox conditions in the glacial aquifer system, northern continental united states. *Water Resources Research* **57** (2021). URL https://doi.org/10.1029/2020wr028207.

[38] Bonte, M. *et al.* Impacts of shallow geothermal energy production on redox processes and microbial communities. *Environmental Science & Technology* **47**, 14476–14484 (2013). URL https://doi.org/10.1021/es4030244. PMID: 24266518, https://doi.org/10.1021/es4030244.

[39] Bonte, M., van Breukelen, B. M. & Stuyfzand, P. J. Temperature-induced impacts on groundwater quality and arsenic mobility in anoxic aquifer sediments used for both drinking water and shallow geothermal energy production. *Water Res.* **47**, 5088–5100 (2013).

[40] Brookfield, A. E. *et al.* Predicting algal blooms: Are we overlooking groundwater? *Science of The Total Environment* **769**, 144442 (2021). URL https://doi.org/10.1016/j.scitotenv.2020.144442.

[41] Bondu, R., Cloutier, V. & Rosa, E. Occurrence of geogenic contaminants in private wells from a crystalline bedrock aquifer in western quebec, canada: Geochemical sources and health risks. *Journal of Hydrology* **559**, 627–637 (2018). URL https://doi.org/10.1016/j.jhydrol.2018.02.042.

[42] Mammola, S. *et al.* Climate change going deep: The effects of global climatic alterations on cave ecosystems. *The Anthropocene Review* **6**, 98–116 (2019). URL https://doi.org/10.1177/2053019619851594. https://doi.org/10.1177/2053019619851594.

[43] Tabilio Di Camillo, A. & Masciopinto, C. Modeling stygofauna resilience to the impact of the

climate change in the karstic groundwaters of south italy. *Water* **14** (2022). URL https://www.mdpi.com/2073-4441/14/17/2715.

[44] Agudelo-Vera, C. *et al.* Drinking water temperature around the globe: Understanding, policies, challenges and opportunities. *Water* **12**, 1049 (2020). URL https://doi.org/10.3390/w12041049.

[45] Torgersen, C. E., Ebersole, J. L. & Keenan, D. Primer for identifying cold-water refuges to protect and restore thermal diversity in riverine landscapes. URL http://pubs.er.usgs.gov/publication/70037945.

[46] Jyväsjärvi, J. *et al.* Climate-induced warming imposes a threat to north european spring ecosystems. *Global Change Biology* **21**, 4561–4569 (2015). URL https://onlinelibrary.wiley.com/doi/abs/10.1111/gcb.13067. https://onlinelibrary.wiley.com/doi/pdf/10.1111/gcb.13067.

[47] Stauffer, F., Bayer, P., Blum, P., Molina Giraldo, N. & Kinzelbach, W. *Thermal use of shallow groundwater* (CRC Press, Boca Raton, FL, 2013).

[48] Bayer, P., Attard, G., Blum, P. & Menberg, K. The geothermal potential of cities. *Renewable and Sustainable Energy Reviews* **106**, 17–30 (2019). URL https://doi.org/10.1016/j.rser.2019.02.019.

[49] Benz, S. A., Bayer, P., Menberg, K., Jung, S. & Blum, P. Spatial resolution of anthropogenic heat fluxes into urban aquifers. *Science of The Total Environment* **524-525**, 427–439 (2015). URL https://doi.org/10.1016/j.scitotenv.2015.04.003.

[50] Epting, J., Müller, M. H., Genske, D. & Huggenberger, P. Relating groundwater heat-potential to city-scale heat-demand: A theoretical consideration for urban groundwater resource management. *Applied Energy* **228**, 1499–1505 (2018). URL https://doi.org/10.1016/j.apenergy.2018.06.154.

[51] Previati, A., Epting, J. & Crosta, G. B. The subsurface urban heat island in Milan (Italy) - a modeling approach covering present and future thermal effects on groundwater regimes. *Science of The Total Environment* **810**, 152119 (2022). URL https://doi.org/10.1016/j.scitotenv.2021.152119.

[52] Benz, S. A., Menberg, K., Bayer, P. & Kurylyk, B. L. Shallow subsurface heat recycling is a sustainable global space heating alternative. *Nature Communications* **13** (2022). URL https://doi.org/10.1038/s41467-022-31624-6.

[53] Schüppler, S., Fleuchaus, P. & Blum, P. Techno-economic and environmental analysis of an aquifer thermal energy storage (ATES) in germany. *Geothermal Energy* **7** (2019). URL https://doi.org/10.1186/s40517-019-0127-6.

[54] Meinshausen, M. *et al.* The RCP greenhouse gas concentrations and their extensions from 1765 to 2300. *Climatic Change* **109**, 213–241 (2011). URL \url{https://doi.org/10.1007/s10584-011-0156-z}.

[55] Zhang, T. Influence of the seasonal snow cover on the ground thermal regime: An overview. *Reviews of Geophysics* **43** (2005). URL https://agupubs.onlinelibrary.wiley.com/doi/abs/10.1029/2004RG000157. https://agupubs.onlinelibrary.wiley.com/doi/pdf/10.1029/2004RG000157.

[56] Zanna, L., Khatiwala, S., Gregory, J. M., Ison, J. & Heimbach, P. Global reconstruction of historical ocean heat storage and transport. *Proceedings of the National Academy of Sciences* **116**, 1126–1131 (2019). URL https://doi.org/10.1073/pnas.1808838115.

[57] von Schuckmann, K. *et al.* Heat stored in the earth system: where does the energy go? *Earth System Science Data* **12**, 2013–2041 (2020). URL https://doi.org/10.5194/essd-12-2013-2020.

[58] World Health Organization. *A global overview of national regulations and standards for*

*drinking-water quality* (World Health Organization, 2021), 2nd ed edn. URL https://apps.who.int/iris/handle/10665/350981. Section: iv, 101 p.

[59] Jones, B. & O'Neill, B. Global population projection grids based on shared socioeconomic pathways (SSPs), downscaled 1-km grids, 2010-2100 (2019). URL https://sedac.ciesin.columbia.edu/data/set/popdynamics-pop-projection-ssp-downscaled-1km-2010-2100.

[60] Gao, J. Downscaling global spatial population projections from 1/8-degree to 1-km grid cells (2017). URL https://opensky.ucar.edu/islandora/object/technotes:553.

[61] Humphreys, W. F. Aquifers: the ultimate groundwater-dependent ecosystems. *Australian Journal of Botany* **54**, 115 (2006). URL https://doi.org/10.1071/bt04151.

[62] Griebler, C. & Avramov, M. Groundwater ecosystem services: a review. *Freshwater Science* **34**, 355–367 (2015). URL https://doi.org/10.1086/679903.

[63] Mammola, S. *et al.* Scientists' Warning on the Conservation of Subterranean Ecosystems. *BioScience* **69**, 641–650 (2019). URL https://doi.org/10.1093/biosci/biz064. https://academic.oup.com/bioscience/article-pdf/69/8/641/29099523/biz064.pdf.

[64] McDonough, L. K. *et al.* Changes in global groundwater organic carbon driven by climate change and urbanization. *Nature Communications* **11** (2020). URL https://doi.org/10.1038/s41467-020-14946-1.

[65] Atawneh, D. A., Cartwright, N. & Bertone, E. Climate change and its impact on the projected values of groundwater recharge: A review. *Journal of Hydrology* **601**, 126602 (2021). URL https://doi.org/10.1016/j.jhydrol.2021.126602.

[66] Hare, D. K., Helton, A. M., Johnson, Z. C., Lane, J. W. & Briggs, M. A. Continental-scale analysis of shallow and deep groundwater contributions to streams. *Nature Communications* **12** (2021). URL https://doi.org/10.1038/s41467-021-21651-0.

[67] Caissie, D., Kurylyk, B. L., St-Hilaire, A., El-Jabi, N. & MacQuarrie, K. T. Streambed temperature dynamics and corresponding heat fluxes in small streams experiencing seasonal ice cover. *Journal of Hydrology* **519**, 1441–1452 (2014). URL https://www.sciencedirect.com/science/article/pii/S0022169414007161.

[68] Power, G., Brown, R. S. & Imhof, J. G. Groundwater and fish—insights from northern north america. *Hydrological Processes* **13**, 401–422 (1999).

[69] Bodri, L. & Cermak, V. *Borehole Climatology* (Elsevier, 2007). URL https://doi.org/10.1016/b978-0-08-045320-0.x5000-5.

[70] Carslaw, H. S. & Jaeger, J. C. *Conduction of heat in solids*. Oxford science publications (Oxford University Press, London, England, 1986), 2 edn.

[71] Turcotte, D. L. & Schubert, G. *Geodynamics* (Cambridge University Press, Cambridge, England, 2014), 3 edn.

[72] Taylor, C. A. & Stefan, H. G. Shallow groundwater temperature response to climate change and urbanization. *Journal of Hydrology* **375**, 601–612 (2009). URL https://www.sciencedirect.com/science/article/pii/S0022169409004004.

[73] Bredehoeft, J. D. & Papaopulos, I. S. Rates of vertical groundwater movement estimated from the earth's thermal profile. *Water Resources Research* **1**, 325–328 (1965). URL https://doi.org/10.1029/wr001i002p00325.

[74] Bense, V. F., Kurylyk, B. L., van Daal, J., van der Ploeg, M. J. & Carey, S. K. Interpreting repeated temperature-depth profiles for groundwater flow. *Water Resources Research* **53**, 8639–8647 (2017). URL https://doi.org/10.1002/2017wr021496.

[75] Brown, J. O. F., Heginbottom, J. A. & Melnikov., E. Circum-arctic map of permafrost and ground-ice conditions, version 2 (2002). URL https://nsidc.org/data/GGD318/versions/2.

642 [76] Gorelick, N. *et al.* Google earth engine: Planetary-scale geospatial analysis for everyone.
643 *Remote Sensing of Environment* **202**, 18–27 (2017). URL https://doi.org/10.1016/j.
644 rse.2017.06.031.

645 [77] Copernicus Climate Change Service. Era5-land monthly averaged data from 2001 to present
646 (2019). URL https://cds.climate.copernicus.eu/doi/10.24381/cds.68d2bb30.

647 [78] Hansen, J. *et al.* Climate simulations for 1880–2003 with GISS modelE. *Climate Dynamics*
648 **29**, 661–696 (2007). URL https://doi.org/10.1007/s00382-007-0255-8.

649 [79] Soong, J. L., Phillips, C. L., Ledna, C., Koven, C. D. & Torn, M. S. CMIP5 models
650 predict rapid and deep soil warming over the 21st century. *Journal of Geophysical Research:*
651 *Biogeosciences* **125** (2020). URL https://doi.org/10.1029/2019jg005266.

652 [80] Huscroft, J., Gleeson, T., Hartmann, J. & Börker, J. Compiling and mapping global
653 permeability of the unconsolidated and consolidated earth: GLobal HYdrogeology MaPS
654 2.0 (GLHYMPS 2.0). *Geophysical Research Letters* **45**, 1897–1904 (2018). URL https:
655 //doi.org/10.1002/2017gl075860.

656 [81] VDI-Gesellschaft Energie und Umwelt (GEU). VDI 4640 - thermal use of the underground
657 (2010).

658 [82] Börker, J., Hartmann, J., Amann, T. & Romero-Mujalli, G. Terrestrial sediments of
659 the earth: Development of a global unconsolidated sediments map database (GUM).
660 *Geochemistry, Geophysics, Geosystems* **19**, 997–1024 (2018). URL https://doi.org/10.
661 1002/2017gc007273.

662 [83] Hartmann, J. & Moosdorf, N. The new global lithological map database GLiM: A
663 representation of rock properties at the earth surface. *Geochemistry, Geophysics, Geosystems*
664 **13** (2012). URL https://doi.org/10.1029/2012gc004370.

[84] Rau, G. C., Andersen, M. S., McCallum, A. M., Roshan, H. & Acworth, R. I. Heat as a tracer to quantify water flow in near-surface sediments. *Earth-Science Reviews* **129**, 40–58 (2014). URL https://doi.org/10.1016/j.earscirev.2013.10.015.

[85] Halloran, L. J., Rau, G. C. & Andersen, M. S. Heat as a tracer to quantify processes and properties in the vadose zone: A review. *Earth-Science Reviews* **159**, 358–373 (2016). URL https://doi.org/10.1016/j.earscirev.2016.06.009.

[86] Davies, J. H. Global map of solid earth surface heat flow. *Geochemistry, Geophysics, Geosystems* **14**, 4608–4622 (2013). URL https://doi.org/10.1002/ggge.20271.

[87] Fan, Y., Li, H. & Miguez-Macho, G. Global patterns of groundwater table depth. *Science* **339**, 940–943 (2013). URL https://doi.org/10.1126/science.1229881.

[88] Fan, Y., Miguez-Macho, G., Jobbágy, E. G., Jackson, R. B. & Otero-Casal, C. Hydrologic regulation of plant rooting depth. *Proceedings of the National Academy of Sciences* **114**, 10572–10577 (2017). URL https://doi.org/10.1073/pnas.1712381114.

[89] Center For International Earth Science Information Network-CIESIN-Columbia University. Gridded population of the world, version 4 (gpwv4): Population density adjusted to match 2015 revision un wpp country totals, revision 11 (2018). URL https://sedac.ciesin.columbia.edu/data/set/gpw-v4-population-density-adjusted-to-2015-unwpp-country-totals-rev11.

[90] Tissen, C., Benz, S. A., Menberg, K., Bayer, P. & Blum, P. Groundwater temperature anomalies in central Europe. *Environmental Research Letters* **14**, 104012 (2019). URL https://doi.org/10.1088/1748-9326/ab4240.

# Acknowledgements

S.A.B. was supported through a Banting postdoctoral fellowship, administered by the Government of Canada. B.L.K. was supported through the Canada Research Chairs program. K.M. was supported by the Margarete von Wrangell-program of the Ministry of Science, Research and the Arts Baden-Württemberg (MWK). We thank Carolin Tissen for sharing data she collected in her study on groundwater temperature anomalies in Europe (90) and the many other people and agencies collecting groundwater temperature data and making it available through (publicly accessible) databases. Without these data, successful validation of our method would not have been possible.

# Author Contributions

S.A.B., B.L.K, and D.J.I. designed the study. S.A.B., B.L.K. D.J.I., G.C.R., Ph.B., K.M., and Pe.B. developed the methodology. S.A.B. prepared all data and code for analysis, and designed figures. D.J.I. designed figure 1. S.A.B., B.L.K., D.J.I., and G.C.R. wrote the manuscript. All authors interpreted results and edited the manuscript together.

# Competing Interests Statement

The authors declare no competing interests.

# Figures

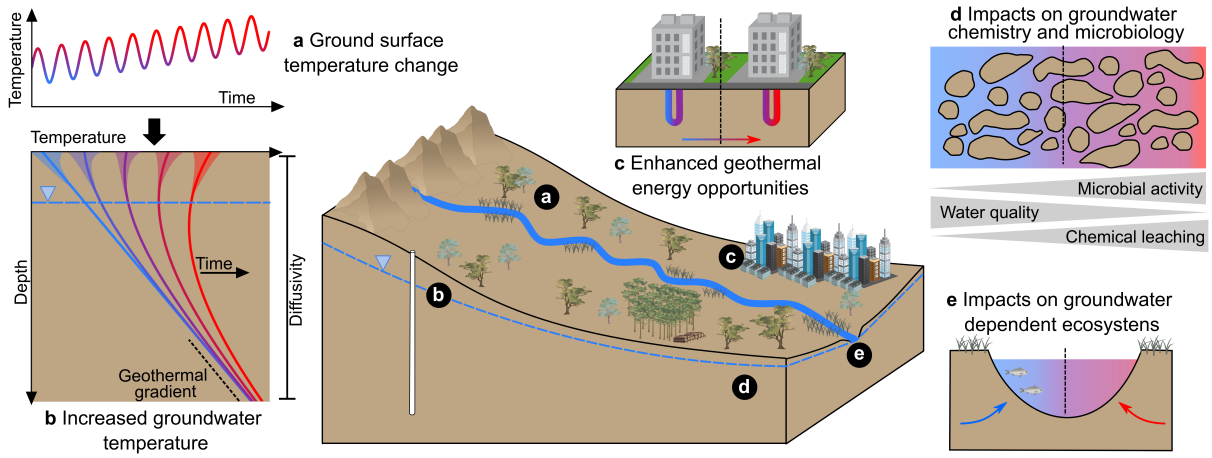


Figure 1: **Processes and impacts related to groundwater temperature changes: a)** increases in surface air and ground surface temperatures drive, **b)** increases in groundwater temperatures that in turn impact, **c)** the geothermal potential for shallow geothermal energy systems, **d)** groundwater chemistry and microbiology which in turn impacts water quality, and **e)** groundwater dependent ecosystems.

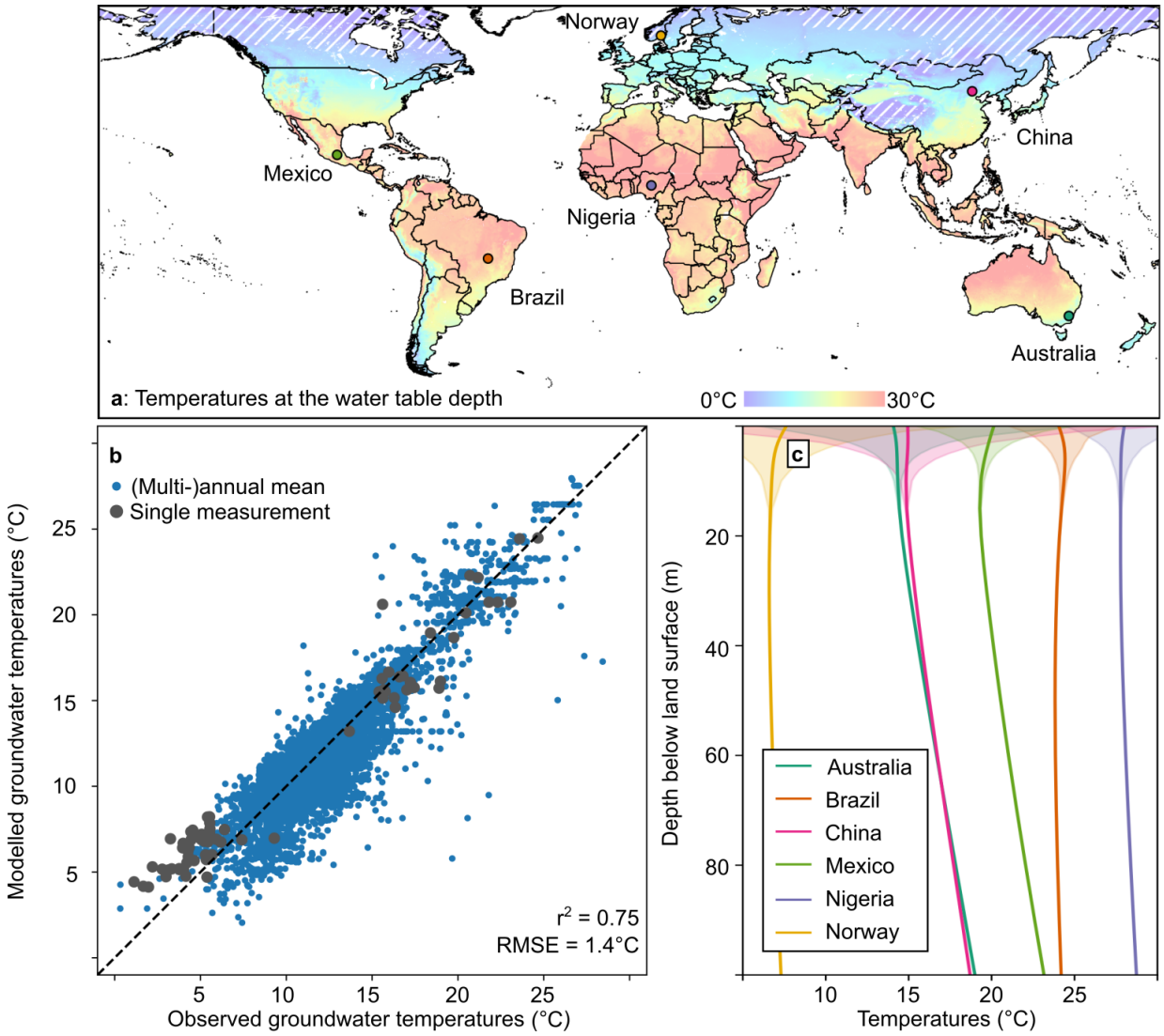


Figure 2: **Current groundwater temperatures. a)** Map of modelled mean annual temperatures at the depth of the water table in 2020. Permafrost regions (75) are hatched to highlight the additional uncertainties of our model in these areas. **b)** Comparison of modelled and observed groundwater temperatures. Blue markers are (multi-)annual mean temperatures observed between 2000 to 2015 at an unspecified depth against modelled temperatures of the same time period at 30 m depth. Gray markers are temperatures of a single point in time vs. modelled temperatures of the same time and depth. **c)** Modelled temperature-depth profiles showing mean annual temperatures and the seasonal envelope for the locations displayed in a).

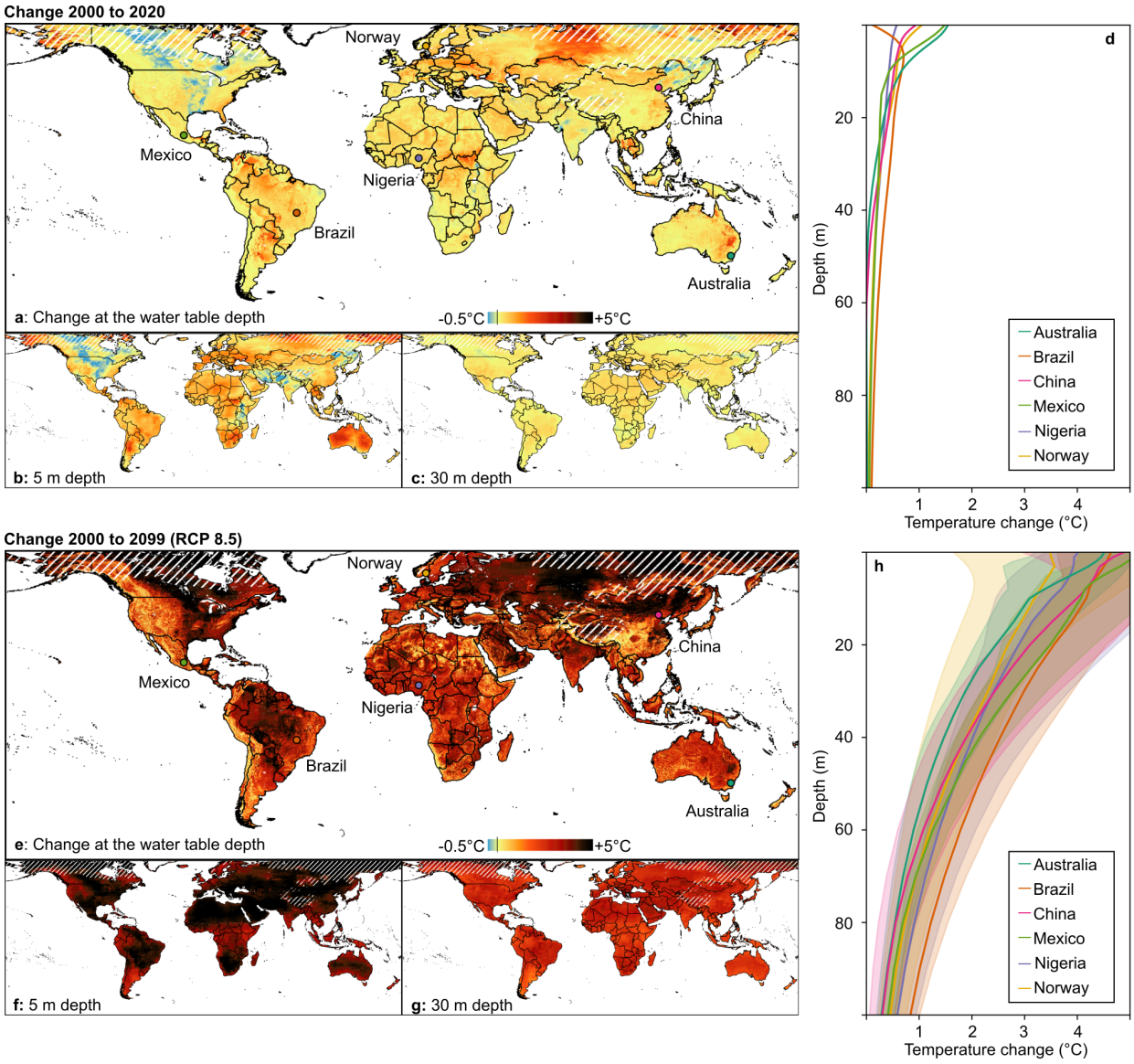


Figure 3: **Change in groundwater temperatures between 2000 and 2020 and between 2000 and 2099 following RCP 8.5. a) - d)** recent (2000 to 2020) changes, **e) - h)** projected (2000-2099) changes. **a)** and **e)** Map of the change in annual mean temperature at the depth of the water table. The line in the legend indicates 0 °C. **b)** and **f)** temperature change 5 m below the land surface, and **c)** and **g)** 30 m below the land surface. In all maps permafrost regions are hatched to highlight the additional uncertainties of our model in these areas. **d)** Change in temperatures between 2000 and 2020, and **h)** difference between 2000 and 2099 as depth profiles for selected locations (see symbols in a and e). Lines in h) indicate median projections, whereas 10th to 90th percentile are presented as shading.

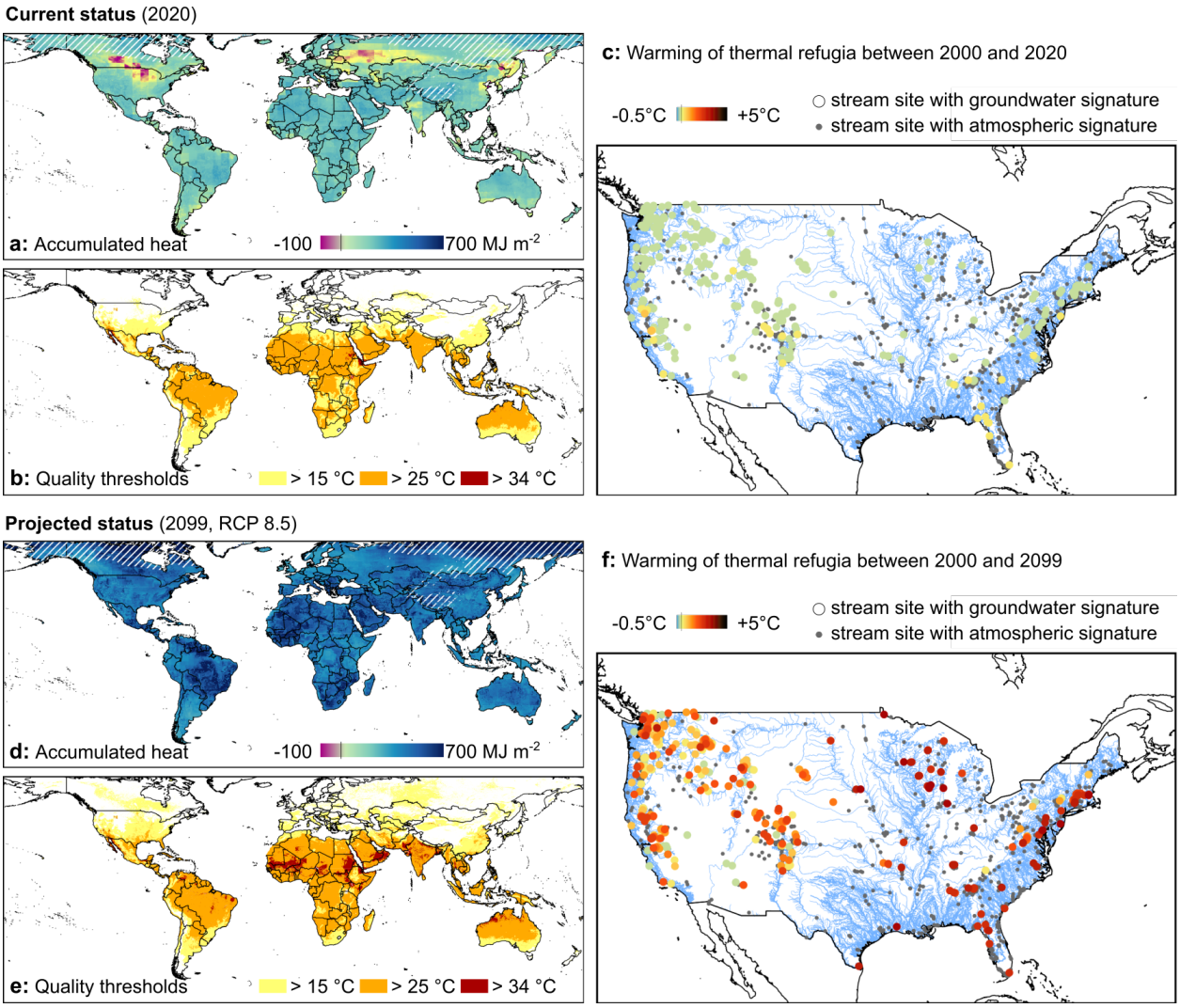


Figure 4: **Implications of groundwater warming. a) - c)** Current status in 2020; **d) - f)** projected status in 2099 under RCP 8.5. **a)** and **d)** Accumulated heat from the surface to 100 m depth. The line in the legend indicates $0 MJm^{-2}$. **b)** and **d)** Map showing locations with maximum monthly GWTs above guidelines for drinking water temperatures (58). **c)** GWT changes between 2000 and 2020 and **f)** between 2000 and 2099 at stream sites with a groundwater signature (66). The line in the legend indicates 0 °C.